Structure Formation and Thermal Stability of Mono- and Multilayers of Ethylene Carbonate on Cu(111) – A Model Study of the Electr....

Article *in* The Journal of Physical Chemistry C · July 2016

DOI: 10.1021/acs.jpcc.6b05012

CITATIONS
3

READS
40

9 authors, including:

Maral Bch
Ulm University
7 PUBLICATIONS **46** CITATIONS
SEE PROFILE

Hanieh Farkhondeh
University of Waterloo
6 PUBLICATIONS **65** CITATIONS
SEE PROFILE

Benedikt Uhl
Ulm University
14 PUBLICATIONS **210** CITATIONS
SEE PROFILE

Joachim Bansmann
Ulm University
128 PUBLICATIONS **2,233** CITATIONS
SEE PROFILE

J. Phys. Chem. C, volume 1196, issue 29, pages 16649-16659, 6/2015,

DOI: 10.1021/acs.jpcc.5b03765

url: http://pubs.acs.org/doi/abs/10.1021/acs.jpcc.5b03765

Reactive Interaction of (Sub)–monolayers and Multilayers of the Ionic Liquid 1–butyl–1–methyl-pyrrolidinium bis(tri–fluoro–methylsulfonyl)imide with Co-adsorbed Lithium on Cu(111)

Florian Buchner,[a] *Maral Bozorgchenani,*[a,b] *Benedikt Uhl,*[a,b] *Hanieh Farkhondeh,* [§,a,b] *Joachim Bansmann,*[b] *and R. Jürgen Behm**[a,b]

[a] Helmholtz Institute Ulm – Electrochemical Energy Storage, Helmholtzstraße 11, D–89081 Ulm,

[b] Ulm University, Institute of Surface Chemistry and Catalysis, Albert–Einstein–Allee 47, D–89081 Ulm,

[§] Present address: WATLab and Department of Chemistry, University of Waterloo, Waterloo, Ontario, N2L 3G1 Canada

Prof. Dr. R. J. Behm
Universität Ulm
Institut für Oberflächenchemie und Katalyse
Albert–Einstein–Allee 47
D–89069 Ulm, Germany
Phone: +49 (0)731/50–25451
Fax: +49 (0)731/50–25452
E–Mail: juergen.behm@uni–ulm.de

ABSTRACT

The ionic liquid (IL) 1–butyl–1–methylpyrrolidinium bis(tri–fluoro–methylsulfonyl)imide [BMP][TFSA] is a promising candidate for improved next–generation rechargeable lithium–ion batteries. We here report results of a model study of the reactive interaction of (sub–) monolayers and multilayers of [BMP][TFSA] with lithium (Li) on Cu(111), employing scanning tunnelling microscopy (STM), X–ray photoelectron spectroscopy (XPS) and Fourier transform infrared spectroscopy (FTIRS) under ultrahigh vacuum (UHV) conditions. Upon post–deposition of Li on [BMP][TFSA] multilayers at 80 K we identified changes in the chemical state of the [TFSA] anion and the [BMP] cation, as well as in the IR absorption bands related to the anion. These changes are most likely due to the decomposition of the IL adlayer into a variety of products like LiF, Li_2S, Li_2O upon anion decomposition and LiN_3, LiC_xH_yN and / or Li_xCH_y upon cation decomposition, where the latter includes cracking of the pyrrolidinium ring. Deposition of Li on [BMP][TFSA] (sub–) monolayer covered surfaces led to similar decomposition patterns, and the same was observed also for the reverse deposition order. Addition of the corresponding amounts of Li to a [BMP][TFSA] adlayer resulted in distinct changes in the STM images, which must be due to the surface reaction. After annealing to 300 K, the core level peaks of the cation lose most of their peak area. Upon further heating to 450 K, the anion is nearly completely decomposed, resulting in LiF and Li_2S decomposition products which dominate the interface.

KEYWORDS: Ionic liquids, Lithium, Li-ion batteries, electrode–electrolyte interface, scanning tunneling microscopy, surface chemistry

Ionic liquids (ILs), which are mostly molten organic salts with a melting point below 100°C, received tremendous attention in both fundamental research and in new applications, ranging from materials science, electrochemistry, catalysis to medical chemistry.[1-4] This is due to their unique physical and chemical properties, which can furthermore be varied widely and adapted to specific applications by making use of the multitude of different anion–cation combinations. Background of the present study is their potential application in the area of electrochemical energy storage, e.g., as solvents in lithium ion and lithium air batteries.[5-7]

The systematic optimization of ILs towards this application requires a fundamental understanding of the processes at the IL | solid interface at the molecular level. Accordingly, numerous studies on the interaction between ILs and solid electrode surfaces have been reported, which were conducted either *in situ,* under electrochemical conditions,[8-13] or *ex situ,* in ultrahigh vacuum (UHV).[14-26] Nevertheless, studies aiming at and resolving details on the adsorption at the IL | metal interface at the (sub–)molecular scale are just at the very beginning.[21-26] This is topic of an ongoing study in our Institute on the interaction of ILs, which are relevant for battery application such as 1–butyl–1–methylpyrrolidinium bis-(tri–fluoro–methylsulfonyl)imide [BMP][TFSA], and well–defined model electrode surfaces (*i.e.*, noble and transition metal surfaces) under ultra high vacuum (UHV) conditions. In previous reports we focused on the self–assembly of the molecules, the intermolecular interactions, the intramolecular conformation and the thermal stability of the adspecies on the surface.[22-26] It has been demonstrated, e.g., that on Ag(111) and Au(111) [BMP][TFSA] adsorbs intact, without decomposition, at least at temperatures below around 400 K, while on Cu(111) the anion decomposes in the temperature range between 300 – 350 K. [26]

Battery electrolytes, however, are mostly complex multicomponent systems which consist of one or more organic solvents (ILs and / or carbonates) and a lithium (Li) salt (e.g. $LiPF_6$, [Li][TFSA]). These components determine formation and properties of the so–called solid|electrolyte interphase (SEI), which is a function determining layer formed at the

electrode|electrolyte interface during initial potential cycling.[27] Molecular scale studies on the interactions between different electrolyte components including ILs have been extremely scarce so far. Kurisaki *et al.* reported X-ray photoelectron spectroscopy (XPS) measurements on a droplet of a mixture of 1–ethyl–3–methylimidazolium bis(trifluoromethylsulfonyl)imide [EMIM][TFSA] and [Li][TFSA] under potential-free conditions, and proposed that the [TFSA] anion is concentrated near the surface, with the lithium ion coordinated by the oxygen atoms of the anion.[28] Very recently, Oschlewski et al. studied the interaction of Li with a 7 nm thick 1-octyl-3-methylimidazolium bis-(trifluoromethylsulfonyl)amide ([OMIM][TFSA]) or [BMP][TFSA] film on a copper foil. XP spectroscopy resolved a variety of reaction products such as LiF, Li_2O and Li_xCH, reflecting the instability of the IL against lithium. In constrast, vapor deposition of the IL on an oxygen passivated lithium layer revealed nearly unaffected anions and partially decomposed cations.[29] Other studies focused on the chemical composition of the SEI after potential cycling, *e.g.*, in [Li][TFSA] and different solvents or polymer electrolyte, employing subsequent *in vacuo* characterization of the SEI by X–ray photoelectron spectroscopy (XPS). Ismail et al. characterized the surface layer formed on a lithium-metal electrode after this had been in contact with a [Li][TFSA] salt doped solid polymer electrolyte. The resulting layer was found to consist of decomposition products of the anion such as LiF, indicated by a F 1s peak with a binding energy (BE) of 685.5 eV, together with compounds of the as-received Li-foil as Li_2CO_3/LiOH and Li_2O.[30] Xu et al. detected a peak at 685.0 eV in the F1s BE range of spectra recorded at the interface between graphite and a lithium|solid polymer electrolyte, which they ascribed to the formation of LiF during the first discharge process. They tentatively attributed this to either originate from the binder and / or from decomposition of [Li][TFSA] salt.[31] They also found further degradation products like Li_2S, S_x, Li_2SO_3 and Li_3N, which fit well into the canon of decomposition fragments proposed by Aurbach et. al..[32] The latter authors suggested that reductive decomposition of [Li][TFSA] during potential cycling may lead to the following compounds: Li_3N, LiF, $C_2F_xLi_y$, Li_2S,

$Li_2S_2O_4$, Li_2SO_3, SO_2CF_x. Nguyen et al. reported on the reductive decomposition of the cation and the [TFSA] anion on a Si–Cu anode during initial cycling to species like SO_x, CF_x, Li_3N and LiF. [33]

Overall, these *in-situ* and *ex-situ* spectroscopic measurements suggested that the formation of the SEI mainly results from a potential–dependent decomposition of the [TFSA] anion during the cycling process. They did not gain, however, direct molecular scale information on the processes going on at the electrode|electrolyte interface. This is topic of the present communication, where we report on the co–adsorption of [BMP][TFSA] and Li and the Li induced decomposition under UHV conditions on a well–defined Cu (111) model electrode surface, employing scanning tunnelling microscopy (STM), X–ray photoelectron spectroscopy (XPS) and Fourier transform infrared spectroscopy (FTIRS). Following earlier studies on the adsorption behavior of the individual components of the electrolyte,[22-26,34] the present work aims at identifying molecular building blocks of the SEI and to unravel the interactions at the model electrode|electrolyte interface for (sub–)monolayer coverage with atomic / molecular resolution. We consider model studies like this and the resulting detailed understanding of the processes at the electrode | electrolyte interface as essential for a systematic improvement of next–generation rechargeable lithium–ion batteries.

2. Results and Discussion

2.1 Pristine adlayers of [BMP][TFSA] and Li

Before exploring the interaction between the co-adsorbed [BMP][TFSA] and Li, both species were separately adsorbed and characterized on Cu(111). A (sub–) monolayer of [BMP][TFSA] was prepared by vapor deposition on the sample held at 80 K and subsequent imaged by STM around 100 K. The images depicted in Figure 1a–f display partly IL covered surfaces at different scales. The surface is covered by a 0.4 ML [BMP][TFSA] adlayer (the monolayer coverage (1 ML) is defined by the number of adsorbed ions in direct contact with the metal surface atoms at saturation). The adsorbed IL species are agglomerated into islands with relaxed dendritic shapes, which are homogeneously distributed over the terraces. In the regions close to steps they start to grow both from the ascending and the descending side of the step edges (Figure 1a-d). Higher resolution images as shown in Figures 1d and 1e illustrate that the islands are composed of round and elliptic protrusions which are arranged in a disordered way with an average nearest neighbor distance of 0.85 ± 0.05 nm, which agrees quite well with the maximum diameter of either an anion or a cation (see also ref [24]) In contrast to [BMP][TFSA] adsorption on Ag(111) and Au(111),[23-25] we did not find any highly ordered 2D crystalline phases. Furthermore, these images do not allow to identify and discriminate between adsorbed anions and cations, which had been possible for adsorption on Ag(111) and Au(111). In the latter cases a round protrusion could be associated with the upstanding alkyl chain of the cation, while two parallel elliptic protrusions were in good agreement with the calculated STM image of the adsorbed anion, specifically with the two CF_3 groups of the anion. Most likely, the different arrangement and possibly also intramolecular conformation of the adsorbed ILs on Cu(111) as compared to those on Ag(111) and Au(111) result from kinetic effects, hindering the adlayer to reach a well ordered, stable configuration.

Second, a small amount of Li was deposited on the Cu(111) substrate held at 80 K and the resulting surface was characterized by STM. The STM micrographs in Figures 2a and b show protrusions which are dispersed over the surface (ρ_{Li} = 0.02 nm^{-2}). These features are very similar to those observed by Simic–Milosevic et al. and by Krull et al. for Li adsorption on Ag(001) and Ag(100) at liquid helium temperature.[35,36] Therefore, they are tentatively attributed to individual Li adatoms or small clusters. A majority of the protrusions exhibits an apparent height of 1.9 ± 0.2 Å, while a minority is slightly higher with 2.6 ± 0.2 Å at the given tunneling conditions. Similar observations were also reported by Simic–Milosevic et al., who assigned the higher features to vertical Li dimers.[35] It should be noted, however, that they could equally well result also from double-layered clusters.

STM images recorded at a magnified scale are shown in Figures 2 c and 2d (the copper atomic lattice is resolved and depicted in Figure 2d). Additional local indentations resolved in these images are attributed to adsorbed oxygen species, which even after careful preparation are still present on the surface at very low concentrations (≤ 0.015 nm^{-2}) and cause a local decrease in the density of states. The full width at half maximum (fwhm) of the dispersed protrusions is 1.4 ± 0.2 nm and 1.7 ± 0.2 nm, respectively, which is much more than expected for a single Li adatom. It may be justified, however, when considering electronic effects and tip effects, due to convolution of the surface feature with the STM tip, which results in an apparently larger size of the imaged feature. From the fact that we observe a decoration of the steps (see Figure 5 centre and Supporting Information (SI 1 and 2)) we assume that the impinging Li atoms can diffuse on the surface over a distance which is at least as long as the terrace width at 80 K. The Langmuir–Gurney model claims a dispersion of Li over the surface due to positively charged Li ions with dominantly repulsive short–range interactions. If the adsorbed species are significantly charged, one would not assume the formation of adsorbed aggregates, but from our STM images we can not distinguish between these two, since due to tip effects even adsorbed atoms may look much larger.

2.2 Li post-deposition on [BMB][TFSA] multilayers (XPS, FTIR)

Prior to the post–deposition of Li, a [BMP][TFSA] film of approximately 6 layers (deposition rate = 0.1 ML / min) was vapor deposited on a Cu(111) substrate held at 80 K and subsequently heated to examine the thermal stability of the [BMP][TFSA] film by FTIRS. The IR spectra, which were successively acquired (t_{ac} = 5min), are presented as difference spectra, with the background spectrum of the [BMP][TFSA] covered sample at 80 K subtracted in Figure 3a. Therefore, these spectra reflect the changes in the vibrational structure of the film due to either decomposition or desorption. Correspondingly, the first spectrum at 80 K shows a featureless line exhibiting no changes. Upon heating, weak bands start to evolve, indicating the onset of thermally induced changes in the adlayer. In the following these bands are more pronounced mainly in the range between 1000 and 1500 cm^{-1}, and successively increase in intensity. It should be noted that from technical reasons no correct temperature readings were possible in this experiments and that the spectra were taken every 5 min, until no changes were visible any more (complete desorption). Because of the pronounced non-linear heating rate this does not correspond to constant temperature steps between the spectra. The most intensive bands are observed at 1062, 1140, 1148, 1218, 1233, 1245, 1330 and 1358 cm^{-1}. Bands with similar wavenumbers were observed in IR spectra of adsorbed multilayers of an IL with identical anion (i.e., 1–butyl–3–methylimidazolium bis(tri–fluoro–methylsulfonyl)imide [BMIM][TFSA]) on Al_2O_3/NiAl(110) recorded at low temperatures and assigned to intact adsorbed molecules.[37,38] The assignment of the [TFSA] related bands in the mid–IR regime has been discussed in detail earlier and the modes attributed to the cation were found to be weak and appear above 1400 cm^{-1}, while the most intense bands in the spectrum were all related to the anion.[39,40] The band around 1062 cm^{-1} is assigned to the asymmetric stretching mode of the S–N–S group ($\nu_{as,SNS}$). The absorption band around 1140 cm^{-1} ($\nu_{s,SO2}$) and that at 1330 and 1358 cm^{-1} ($\nu_{as,SO2}$) are attributed to the symmetric and asymmetric stretchin modes of SO_2, respectively. Finally, the three bands at 1218 ($\nu_{as,CF3}$), 1233 ($\nu_{s,CF3}$) and 1245 cm^{-1}

represent the fingerprint of the CF_3 stretching modes. Thus, all features resolved in our experiment are attributed to [BMP][TFSA], demonstrating a loss of the IL upon warm-up. Our previous XPS study revealed that (sub-)monolayers of [BMP][TFSA] adsorb intact on Cu(111) at 80 K with a balanced ratio of anions to cations.[26] Furthermore, temperature dependent STM and XPS measurements demonstrated that the [TFSA] anion decomposes during annealing in the temperature interval between 300 and 350 K into anion fragments such as S_{ad}, SO_x, CF_3.[26] Interestingly, we found no bands related to the latter species in the current FTIRS measurements, in contrast to findings in STM and XPS measurements, which may be explained either by a too small amount of residues on the surface or by species which are not infrared active. Finally, the dectected bands are most likely related to multilayer desorption.

In the following experiments, both FTIRS and XPS measurements were performed on the same sample under identical conditions in the same UHV chamber. XP spectra of the neatly adsorbed [BMP][TFSA] film at 80 K were recorded first. Second, FTIR spectra were recorded both on the same Li-free [BMP][TFSA] film, followed by a second measurement after post-deposition of Li to resolve the Li-induced changes. In the third step, also XP spectra were recorded on the [BMP][TFSA] + Li covered sample. To begin with, we show isothermal FTIRS experiments at 80 K, monitoring the changes in the IR spectrum upon subsequent co-deposition of Li on the [BMP][TFSA] multilayer film, which was prepared as described before. Difference spectra (baseline corrected), obtained using the spectrum recorded on the Li-free multilayer film as background spectrum, show the same vibrational modes (S–N–S, SO_2 and CF_3) as found upon heating (Figure 3b). These changes at 80 K clearly point toward a Li induced decomposition of the [TFSA] anion already at the low deposition temperature.

Subsequently to the FTIRS measurements, the [BMP][TFSA] multilayer + Li covered Cu(111) sample was transfered to the XPS measurement station at constant temperature and

the chemical state of the multilayer was probed. Figure 4 shows a comparison of representative F 1s, N 1s, C 1s and S 2p core level spectra, which were recorded once on the Li-free multilayer (spectra at the bottom of each panel) and once after post-deposition of Li (spectra on top of each panel). The F 1s region (Figure 4a) reveals a single peak (F_{anion}) at 689.0eV which originates from the [TFSA] anion. After co–deposition of Li, the initial [TFSA] peak (F_{anion}) slightly shifts by +0.2 eV to higher binding energy and a new peak is formed at the low binding energy (BE) side at 685.5 eV, which in agreement with previous reports is assigned to LiF.[31] This assignment is corroborated by observations in the Li 1s region (Supporting Information (SI 3)), where a LiF peak evolves at 56.0 eV. This is close to the BE of the Li 1s peak of ~55.9 eV reported for the alkali metal halide LiF.[41] In combination, these data indicate that fluorine atoms are abstracted from the [TFSA] anion upon Li post–deposition at 80 K. Note that also other Li containing components like Li_2O, Li_2S, Li_3N might contribute to the Li 1s peak, which will be discussed in the following.

The N 1s signal of the as–deposited IL film reveals two components, which are related to the nitrogen atoms of the cation (N_{cation}) at 402.4 eV and to that of the anion (N_{anion}) at 399.5 eV, respectively (Figure 2b). The N_{cation} : N_{anion} intensity ratio is around one, reflecting a balanced ratio of cations to anions in the multilayer film. After post–deposition of Li, the initial [BMP][TFSA] peaks (N_{cation} and N_{anion}) shift by around + 0.8 eV to 403.1 and 400.4 eV, respectively. Additionally, a new peak appears at the low binding energy side at 397.9 eV, mainly at the expense of the N_{cation} related peak intensity, which must therefore arise predominantly from a reaction product of [BMP] with Li. But also the intensity of the N_{anion} signal decreases slightly, which indicates that the new peak includes also contributions from a reaction product of [TFSA] and Li. This binding energy (397.9 eV) is characteristic for Li_3N, which based on electrochemical measurements was suggested as [TFSA] decomposition product by Xu et al. and Aurbach et al..[31,32] On the other hand, Oschlewski et al. [29] who had post-deposited Li on a 7 nm thick [BMP][TFSA] multilayer film adsorbed on a copper foil

(deposition at room temperature) and found a very similar peak, assigned this new peak to a chain-like LiC_xH_yN structure, which was created by an opening of the pyrrolidinium ring. Thus, the new peak at 397.9 eV could either be ascribed to Li_3N or LiC_xH_yN.

The C 1s XP signal in Figure 4c exhibits three peaks at 285.4, 286.6 and 293.1 eV respectively. The peak referred to as C_{alkyl} (285.4 eV) is related to the two carbon atoms in the pyrolidinium ring and the three carbon atoms in the butyl chain.[17,18,23,24] The C_{hetero} peak (286.6 eV) is due to the four carbon atoms with nitrogen neighbors, and the C_{anion} feature (293.1 eV) is related to the two carbon atoms in [TFSA]. The nominal ratio of these carbon atoms of 5 : 4 : 2 is close to the experimentally determined ratio of the peak areas. Hence, also the C 1s signals reflect an anion to cation ratio of 1 : 1, indicative of molecular adsorption of anions and cations. After addition of Li, the C_{anion} peak decreases by 40% in intensity and shifts to a marginally higher BE (+0.15 eV). The C_{hetero} and C_{alkyl} peaks shift by 0.5 eV to higher BE and decrease by 37% and 18 %, respectively. In addition to the decrease of the N_{cation} signal, the pronounced decrease of the C_{hetero} signal points toward a reaction of [BMP] and Li on the copper surface. A similar decrease of the peak area of C_{anion} and of the ratio between C_{hetero} : C_{alkyl} was recently found by Olschewski et al. in the XP spectra of thick [BMP][TFSA] films, which were deposited at room temperature on a lithium film, and attributed to a pyrrolidinium ring breakup.[29]

The S 2p XP spectrum shows a doublet with features at 168.8 and 170.2 eV, which is associated with the sulfone ($-SO_2$) group in the [TFSA] anions (S_{anion}). Upon post–deposition of Li the main peak [TFSA] broadens and a new doublet appears at 161.6 and 163.0 eV respectively. The latter could either be assigned to adsorbed atomic sulphur or to Li_2S. The broadened main peak could also include two doublets to obtain a satisfactory fit: the initial [TFSA] doublet (S_{anion}) at 168.8 and 170.2 eV plus an additional doublet at 167.6 and 168.9 eV. From the XP spectra we can not distinguish between these two possibilities. XP S 2p peaks with similar BEs arising from [TFSA] anion decomposition during charging and

discharging on sulphur cathodes were observed by Diao et al. and related to either S–O, S–S or Li–S bond containing species.[42]

The O 1s region exhibits a characteristic peak at 532.8 eV, which is associated with the oxygen atoms in the [TFSA] anions (O_{anion}), plus a weak peak at 530.8 eV which results from oxygen of the tantalum sample holder (Supporting Information (SI 3)). Addition of Li results in the evolution of two more peaks at 531.6 and 529.1 eV, respectively, which we assign to LiOH and Li_2O as reaction products of [TFSA] and Li. Here, we follow Oschlewski et al., who observed similar new peaks upon co-deposition of Li and a 7 nm thick [OMIM][TFSA] film on a Li foil at room temperature and assigned them to LiOH and Li_2O species.[29] Overall, the XPS core level spectra for [BMP][TFSA] multilayers reveal that upon addition of Li the [TFSA] anions decompose into LiF, Li_2O, Li_2S and / or atomic sulphur species and probably other sulphur containing components like $Li_2S_2O_4$, Li_2SO_3, or $LiSO_2CF_3$, in good agreement with the [Li][TFSA] degradation mechanism suggested by Aurbach et al.,[32] In addition, our data suggest that the pyrrolidinium ring of the [BMP] is opened and LiN_3 or LiC_xH_yN species are formed, which, in turn, agrees well with the interpretation given by Oschlewski et al..[29]

2.3 Li post-deposition on [BMB][TFSA] (sub-) monolayers (XPS)

After having characterized the adsorption behavior of both components on Cu(111), Li was successively post–deposited on a 0.6 ML [BMP][TFSA] pre–covered surface at 80 K. Subsequently, the surface was analyzed by XPS. Representative F 1s and Li 1s as well as S 2p and C 1s core level spectra recorded on the sample held at 80 K are shown in Figures 5 (F 1s, Li 1s) and 6 (S 2p and C 1s). In this coverage regime, the N 1s peak is superimposed on a background feature which can hardly be removed because of the low coverage of adsorbed N atoms; therefore the N 1s signal is not discussed in the following. In order to calibrate the approximate amount of post–deposited Li, three different Li doses were vapor deposited onto the pristine Cu(111) surface at 100 K and characterized by STM at 100 K as shown in the

images next to the XP spectra. The corresponding densities of Li surface features, ρ_{Li} were evaluated as ρ_{Li} = 0.02 nm^{-2}, ρ_{Li} = 0.05 nm^{-2} and ρ_{Li} = 0.07 nm^{-2}. Due to the unknown mean number of Li atoms per Li feature an absolute Li coverage can not be given. On the copper surface with the highest Li particle density the XP Li 1s region was recorded (spectrum at the bottom of Figure 5) revealing a single Li peak centered at 55.1 eV.[43] The peak position at 55.1 eV is indicative of metallic Li on Cu(111), which is supported also by the observation of a similar BE for a sputtered Li foil, where the native film had been largely removed (see Supporting Information (SI 4)).

Now we concentrate on the changes of the F 1s signal upon post–deposition of Li. After deposition, the 0.6 ML [BMP][TFSA] (sub–) monolayer film reveals a single peak (F_{anion}) at 689.1 eV, which is related to the CF_3 groups of [TFSA] (Figure 5a). After a first Li dose the initial [TFSA] peak F_{anion} shifts to higher BEs and an additional small peak emerges at 685.8 eV (Figure 5b). The F_{anion} peaks shifts by +1.1 eV to 690.2 eV. After a second dose of Li (Figure 5c) the intensity of the new peak at the low binding energy side (now located at 686.4 eV) increased and again shifted by +0.65 eV with respect to its previous position (Figure 5b). In addition, the original F_{anion} signal further decreased and shifted by an additional +0.2 eV to 690.4 eV. After a third dose of Li (Figure 5 d), the new F 1s peak continued to grow and again shifted by +0.3 eV to now 686.7 eV. At this point it exhibits nearly the same intensity as the F_{anion} peak, which has further decreased and shifted by +0.25 eV to 690.65 eV. The changes of the total F 1s peak intensity upon post-deposition of Li at 80 K are insignificant. The new F 1s signal appears several eV at lower BE than the initial [TFSA] peak (F_{anion}) peak, which indicates that the organic fluorine compound in the [TFSA] anion is transformed into a highly ionic inorganic LiF compound as we had already suggested after post-deposition of Li to [BMP][TFSA] multilayers at 80 K. Interestingly, the LiF signal appears narrower than the initial [TFSA] peak (F_{anion}), instead of the full width half maximum (fwhm) of around 2.4 eV obtained for Li-free [TFSA] the fwhm of the new peak is only

around 1.8 eV (Figures 5c and 5d). We tentatively explain this by a broadening of the [TSFA] related peak, which may result, *e.g.*, from different adsorption sites of the [TFSA] species. In contrast, for LiF we assume a strong adsorbate–substrate coupling, where the molecules bind to identical adsorption sites, which results in a lower fwhm.

Additional XPS measurements shown in the Supporting Information (SI 5) revealed that the characteristic formation of a LiF related species does not depend on the sequence of [BMP][TFSA] and Li deposition. Spectra recorded on a surface prepared by Li pre-deposition and subsequent [BMP][TFSA] deposition closely resemble those shown in Figure 5d, which were recorded on a surface generated by [BMP][TFSA] pre-deposition followed by Li post-deposition at 80 K. In particular, the spectra show the [TFSA] related F 1s peak (F_{anion} peak, 690.5 eV) and also the LiF related F 1s peak at the low binding energy side (686.2 eV), which is absent for pure adsorbed [BMP][TFSA]. Only the intensity of the LiF related F 1s peak was found to be slightly smaller when Li was pre-deposited, which could originate from a reaction of adsorbed Li on Cu(111) with residual gases in the UHV chamber in the time period before post-deposition of [BMP][TFSA]. In conclusion, the reaction between the adsorbed [TFSA] anion and adsorbed Li on Cu(111) at 80 K occurs independent of the order of the deposition processes.

Next we will evaluate changes in the S 2p and C 1s spectral ranges upon sequential Li post-deposition and annealing. For the [BMP][TFSA] (sub–) monolayer the S 2p region displays a doublet at 168.9 and 170.3 eV, which is due to the sulphur of the adsorbed [TFSA] species (S_{anion}) (Figure 6a). In the corresponding C 1s spectrum we find three peaks at 285.2, 286.5 and 292.9 eV (C_{alkyl}, C_{hetero}, C_{anion}), respectively. The peak areas exhibit the 5 : 4 : 2 ratio of atoms with equivalent atomic neighbors in [BMP][TFSA] as described in Figure 4c for multilayer films. After deposition of a first dose of Li (ρ_{Li} = 0.05 nm^{-2}, see Figure 5)), two new doublets evolve in the S 2p region on the expense of the initial [TFSA] doublet peak S_{anion}. In addition to loosing intensity (-40 %), the latter also shifts by +0.7 eV to 169.6 eV and

171.0 eV, respectively (Figure 6b). The new doublet with the S $2p_{3/2}$ peak at around 166.2 eV exhibits a rather low intensity; based on its binding energy it could be related to $Li_2S_2O_4$, Li_2SO_3, or $LiSO_2CF_3$ type intermediate species. The other new doublet at 162.0 and 163.4 eV, respectively, is attributed to adsorbed sulphur (S_{ad}) or Li_2S. For comparison the S 2p binding energies of different sulphur containing species[44-46] are listed in a Table in the Supporting Information (SI 6). The total changes in S 2p peak area, however, are small (-11 %), indicating that the losses due to S desorption are small. In the C 1s region, the most significant change is the loss of intensity of the C_{anion} peak, which drops by ~40% and shifts by +1.1 eV to 294.05 eV. In addition, the C_{alkyl} and C_{hetero} signals are shifted by around +1.6 and 1.4 eV, respectively, to 286.9 and 288.1 eV. This shift goes along with a decrease of the C_{hetero} : C_{alkyl} ratio from 0.8 to 0.64 (– 16 %) due to an increase of the intensity of C_{alkyl} and a decrease of C_{hetero}, which even considering possible errors in the fit procedure is significant, indicative for a reaction of [BMP] and Li on the copper surface. Very similar changes in the peak area of C_{anion} and the ratio between C_{hetero} : C_{alkyl} were found in the XP spectra of multilayers of [BMP][TFSA], which were deposited either on a copper foil or on a lithium film at room temperature; the changes observed in the latter case were attributed to an opening of the pyrrolidinium ring.[30] Furthermore, at 284.5 eV a new low intensity peak appears in the BE region characteristic for hydrocarbons or carbon bound to lithium (Li_xCH_y). The total C 1s peak area remains more or less constant. After deposition of a second dose of Li (ρ_{Li} = 0.07 nm^{-2}), the [TFSA] related S 2p doublet S_{anion} shifts by another + 0.2 eV to 169.8 and 171.2 eV, respectively, and decreases by another 20 % in intensity (Figure 6c). Also the doublet with the S $2p_{3/2}$ peak at around 166.2 eV fades, while the doublet related to S_{ad} / Li_2S species at 162.2 and 163.6 (+ 0.2 eV) increases in intensity, becoming almost as intense as that related to [TFSA]. The total S 2p peak area, however, changes very little. In the C 1s region, the C_{anion} signal decays in total by 55 % of the initial peak area and also shifts by + 0.25 eV to 294.3 eV. A similar shift is also observed for all other peaks in the C 1s range. The C_{hetero} : C_{alkyl} ratio

decreases moderately, while the shoulder at the low binding energy side at 284.5 eV grows slightly. The total C1s peak area nearly does not change.

In general, the XP spectra of adsorbed (sub-)monolayers of [BMP][TFSA] on Cu(111) exhibit a distinct shift of all peaks to higher binding energies upon post-deposition of Li; the binding energy shifts are summarized in a Table in the Supporting Information (SI 7). A local coordination of Li to the IL in the inital state can not account for the observed shifts for all elements and, even more, it also is not plausible that coordination of Li leads to a general BE increase. Thus, we rule out initial state effects and assume that the observed BE shifts must originate from other (electronic) effects.

2.4. Li post-deposition on [BMP][TFSA] (sub-) monolayers (STM)

Next we focus on structural aspects of the coadsorbed species as evaluated by STM for 0.4 ML [BMP][TFSA] and post–deposited Li. The STM images in Figure 7a–d reveal marked differences compared to adsorbed [BMP][TFSA] on Cu(111) (see Figure 1). Now islands are observed with a contrast inversion of the inner part under similar tunneling conditions as applied before and an additional decoration of the perimeter by a sequence of equidistant protrusions with a distance of around 1 nm. The island exhibit oblong and elliptical shapes and start to grow both at the ascending and descending side of the steps. In the high–resolution STM images in Figures 7c and d even molecular features (dots) are visible in the inner part of the islands, whose exact nature, however, is not yet clear. Furthermore we recognized a standing wave pattern in between the islands which is created by the adsorbate islands on the surface acting as barrier that scatter surface–state electrons. Most interestingly, independently of the amount of co–deposited Li (ρ_{Li} = 0.02 - 0.07 nm^{-2}), we never observed Li as shown in Figure 2 in between the [BMP][TFSA] islands; therefore we assume that statistically impinging Li atoms hit the surface and diffuse until they interact with the adsorbed IL. Thus the protrusions located at the perimeter of the islands are tentatively

assigned to Li containing molecular entities. A more definite assignment is not possible at present. Interestingly, the inner part of the islands appears lower in the STM images than the surrounding Cu(111) surface, which differs from the higher appearance of [BMP][TFSA] islands in the absence of Li, indicating that the adsorbed Li has modified also the inner part of the islands. This is supported also by new structural features in these regions (see Figs. 7c,d).

2.5 Thermal decomposition of pure and Li containing [BMP][TFSA] (sub-) monolayers

In order to elucidate temperature induced changes and to move towards more realistic conditions, the [BMP][TFSA] + Li covered surface was slowly heated to room temperature. Upon annealing to 300 K, the intensity of the XP signals changes only slightly. The F_{anion} signal shifts back to 689.8eV (–0.85 eV), the LiF peak shifts by the same amount to 685.9 eV. Upon annealing to around 450 K, the F_{anion} signal has almost disappeared, with a weak state remaining at around 689.15 eV. The LiF related peak (now at 686.2 eV) has increased further and now dominates the spectrum. Finally, at 450 K the total F 1s peak area decreases moderately by 9 % compared to the peak area at room temperature. From the fact that the LiF related F 1s peak grows upon heating we conclude that the transformation into that species is kinetically hindered at lower temperatures.

After annealing to 300 K, the peak areas in the S 2p region remain relatively similar (Figure 6 d), except for a back-shift in BE by –0.7 eV to 169.1 and 170.5 eV and 161.5 and 162.9 eV, respectively. We assume that the unusual backshift of the XP peaks upon anealing can not be explained by initial state effects and must therefore result from other electronic effects. In contrast, the peak area of the C 1s signal decreases significantly upon annealing to 300 K (- 60 %), which is mainly related to a decrease of the peak area of the cation related signals (C_{alkyl} and C_{hetero}) indicating that much of the carbon of the cation desorbed. Indeed, also Oschlewski et al. observed that the C 1s peaks of the cation of [OMIM][TFSA] lose about 84% of their intensity when Li is post-deposited at room temperature on a 7 nm thick [OMIM][TFSA] film

adsorbed on a copper foil. After annealing to 450 K, mainly S_{ad} / Li_2S persist with S 2p peaks at 161.3 and 162.7 eV respectively (Figure 6e). The total peak area decreased a little by 16 % compared to room temperature.

To demonstrate the impact of the post-deposited Li we also show temperature dependent XP F 1s spectra of a Li-free [BMP][TFSA] adlayer (0.4 ML) in Figure 5g and h. Figure 5g shows the intact adsorbed adlayer on Cu(111) at 80 K and Figure 5h that obtained upon heating to 300 – 350 K. The shift of the F_{anion} signal to lower binding energies (688.2 eV) was associated with the decomposition of the anion to $CF_{3,ad}$ by Uhl et al..[26] The thermal evolution of the XP S 2p and C 1s signals for the Li-free surface is shown in Figure 6f and g. Figure 6f shows XP spectra of the intact adsorbed adlayer on Cu(111) at 80 K and Figure 6g spectra recorded upon heating to 300 – 350 K. Upon annealing, the S 2p spectrum exhibits new peaks, which following our earlier work[26] are attributed to surface decomposition products. The main new doublet peak at 168.0 and 166.8 eV is attributed to SO_x and that at 162.5 and 161.3 eV to S_{ad}. In the C 1s region, the C_{anion} signal shifts by 1.1 eV to lower BE (291.6 eV), which is most likely due to the formation of $CF_{3,ad.}$[26] Note that the latter decomposition products of the Li-free [BMP][TFSA] were not observed upon annealing a [BMP][TFSA] + Li adlayer. Instead, in the latter case Li_2S and LiF dominate the interface and we see a massive Li-induced loss of carbon from the cation, which did not occur in the absence of Li. The distinct difference again illustrates a clearly modified interface with different surface decomposition products of the Li-free [BMP][TFSA] adlayer (SO_x, S_{ad}, CF_3) compared with the [BMP][TFSA] + Li adlayer (LiF, Li_2S) upon annealing to and slightly above room temperature. The resulting surface morphology of a Cu(111) surface covered by 0.4 ML of [BMP][TFSA] (deposition at 80 K) after post-deposition of Li, heating to 450 K and subsequent cool down to around 100 K is illustrated by the large scale STM images in Figure 8 (XP spectra of the F 1s and S 2p region recorded on the same surface are shown in the Supporting Information (SI 8)). The STM images display large islands, which are homogeneously distributed on the terraces. Some of

them are attached to the step edges, both at the ascending and descending side. Furthermore, the steps are decorated by lines of small protrusions. The additional heating procedure as compared to the surface imaged in Figure 7 results in larger island structures, reflecting the thermal mobility of the adspecies during annealing, Furthermore, the mean height of these islands (1.6 Å) and its variation (± 0.3 Å) indicate that they are due to adsorbed features and do not result from three-dimensional structures, *e.g.*, of inorganic compounds. Details of the internal structure of the islands, howver, could not be resolved so far.

4. Conclusions

Aiming at a more detailed understanding of the processes going on at electrode surfaces during the formation of the solid|electrolyte interphase we have investigated the interaction of multilayers and (sub–) monolayers of the ionic liquid [BMP][TFSA] and Li on a Cu(111) model electrode by a combination of STM, XPS and FTIRS measurements. This model study, which was performed under UHV conditions, led to the following conclusions:

1. Multilayers and (sub–) monolayer [BMP][TFSA] films are found to adsorb intact at temperatures below 200 K. (Sub–) monolayers of [BMP][TFSA] are forming islands with relaxed dendritic shapes. Adsorbed Li is identified as small isolated protrusions on Cu(111) at 80 K, which are attributed either to individual Li adatoms or to small aggregates.

2. The interaction of multilayer [BMP][TFSA] films with post–deposited Li leads to decomposition of anions even at 80 K, as indicated by FTIR difference spectra. This is confirmed by XPS measurements, which reveal a decay of signals typical for the [TFSA] anions and the formation of new species such as LiF, S_{ad} and/or Li_2S. The reactive decomposition of the [BMP] cations, reflected by an intensity decay of the XP N 1s signal, leads to the formation of new adspecies, *e.g.*, adsorbed Li_3N or LiC_xH_yN species.

3. Post–deposition of Li on sufaces covered by (sub–) monolayers of [BMP][TFSA] causes significant changes in the adlayer even at 80 K. Structural changes are manifested by a contrast inversion of the interior of the islands and a decoration of their perimeter by round protrusions. Coexistent isolated Li was never observed, indicating that Li adatoms are sufficiently mobile to reach IL adlayer islands in their vicinity and react with the IL forming Li containing molecular entities.

4. Based on XPS post-deposition of Li this is connected with decomposition of the adsorbed [TFSA] anions, leading to LiF and S_{ad} and/or Li_2S surface species. At 80 K, however, this process is kinetically hindered, and occurs only to a limited extent. The reactive decomposition of the adsorbed cation upon Li post-deposition is indicated by changes in the C 1s signal.

5. The presence of Li on the surface causes drastic changes in the thermally activated decomposition pattern of [BMP][TFSA] (sub–) monolayers on Cu(111). Annealing [BMP][TFSA] films without Li present on the surface leads to the formation of mainly $CF_{3,ad}$, $SO_{x,ad}$, S_{ad} and other carbon containing adspecies, whereas annealing the [BMP][TFSA] adlayer in the presence of co-adsorbed Li results in mainly LiF and sulphur containing components (S_{ad} and / or Li_2S surface species), while the initial [BMP] and [TFSA] signatures disappear. Carbon containing species decrease at ≥300 K and nearly completely disappear at 450 K.

Overall, the study gained detailed insight into the Li induced reactive decomposition processes of the [BMP][TFSA] adlayer and also in the nature of the resulting decomposition products, while the structural characterization of the Li induced changes of (sub-) monolayers of [BMP][TFSA] by STM is hindered by the absence of ordered structures on Cu(111), as they were observed on other substrates such as on Ag(111). Further efforts will

concentrate on the interaction of Li and adsorbed ILs on more realistic and battery relevant substrates such as TiO_2 or graphite.

5. Experimental Methods

The experiments were carried out in a commercial ultrahigh vacuum (UHV) system (SPECS GmbH) with a base pressure of 2×10^{-10} mbar. It consists of two chambers, one containing an Aarhus type STM/AFM system (SPECS Aarhus SPM150 with Colibri sensor), which is capable of measurements in a temperature range of 90 K and 370 K by cooling with LN_2 and resistive heating, the other one is equipped with an X–ray source (SPECS XR50, Al-K_α and Mg-K_α) and a hemispherical analyzer (SPECS, DLSEGD–Phoibos–Has3500) for XPS measurements.

The Cu(111) single crystal was purchased from MaTeck GmbH (purity 5N). It has a hat shaped form with a diameter of 9 mm, one side is polished with a roughness of the (111) surface smaller than 30 nm and an orientation accuracy of $< 0.1°$. The ionic liquid [BMP][TFSA] was purchased from Merck in ultra pure quality. The Cu(111) surface was cleaned by Ar^+ ion sputtering (1 kV) and heating to 820 K with the manipulator head simultaneously being cooled by LN_2.With this procedure atomically flat terraces (with the long terrace side of a few hundred nanometers and the short side up to around 100 nm) with a few surface cavities, which we attribute to small amounts of adsorbed oxygen ($\rho \leq 0.016$ nm^{-2}), were obtained. This amount is by far too small to be detected by XPS. LN2 cooling of the manipulator head while annealing the copper substrate to ~ 820 K was the key to significantly reduce the amount of these residues. Thereby it was kept attention that the head was continuously hold below 270 K during annealing.

The ionic liquid was filled into a quartz crucible, which was mounted in a Knudsen effusion cell (Ventiotec, OVD–3). The IL was then degassed for at least 24 hours under UHV

conditions at room temperature, followed by several hours of degassing at up to 400 K. The quartz crucible itself was also baked prior to use at 870 K in UHV. The cleanness of the IL vapor was tested with a quadrupole mass spectrometer (Pfeiffer HiQuad QMA 400). To generate IL adlayers on the Cu(111) surface the IL was evaporated at a temperature of the IL source of 450 K. Under these conditions the deposition rate was around 0.1 ML min^{-1}.

Lithium metal dosing was accomplished with an alkali getter source, a Li dispenser, which was purchased from SAES Getters. Exposures were made by resistively heating the source (7.0 A, 1.1 V) in line-of-sight of the LN_2 cooled Cu(111) sample (80 K) from a distance of around 6 cm.

STM measurements were performed in constant current mode with currents between 15 pA and 50 pA, bias voltages between 0.1 V and 1.5 V (applied to the sample).

For XPS measurements we used an Al K_α X–ray source (1486.6 eV), operated at a power of 250 W (U = 14 kV, I = 17.8 mA). The spectra were recorded at a pass energy of 100 eV at grazing emission (80° to the surface normal). We note that the IL adlayers are sensitive to beam damage upon extended irradiation. In the period of a few hours we observed a moderate intensity decrease of the IL related peaks. Therefore the duration of the XPS measurements was limited to one to three scans per element (a few minutes), respectively.

For the fitting of the XP spectra in Figure 4 a simultaneous fit of background (Shirley + slope) and signal was used, applying an asymmetric Pseudo-Voigt-type function[47] while in Figures 5 and 6, the background was first subtracted.

The FTIR spectra were recorded at incidence and detection angles of 7°with respect to the surface plane at a spectral resolution of 2 cm^{-1}, co-adding interferograms over a period of 5 min per spectrum, using a Bruker 70v spectrometer equipped with a liquid nitrogen cooled MCT detector. The absorbance was calculated as $A = \log(R_0/R)$, with R_0 representing the reflected intensities of the bare Cu surface or of the [BMP][TFSA] adlayer at ~80 K as

indicated in the Figure Captions, while R describes the measured reflected intensity in the respective experiments, *i.e.*, after deposition of [BMP][TFSA] or at elevated temperature, respectively. This results in positive bands for increased absorbance.

Figures

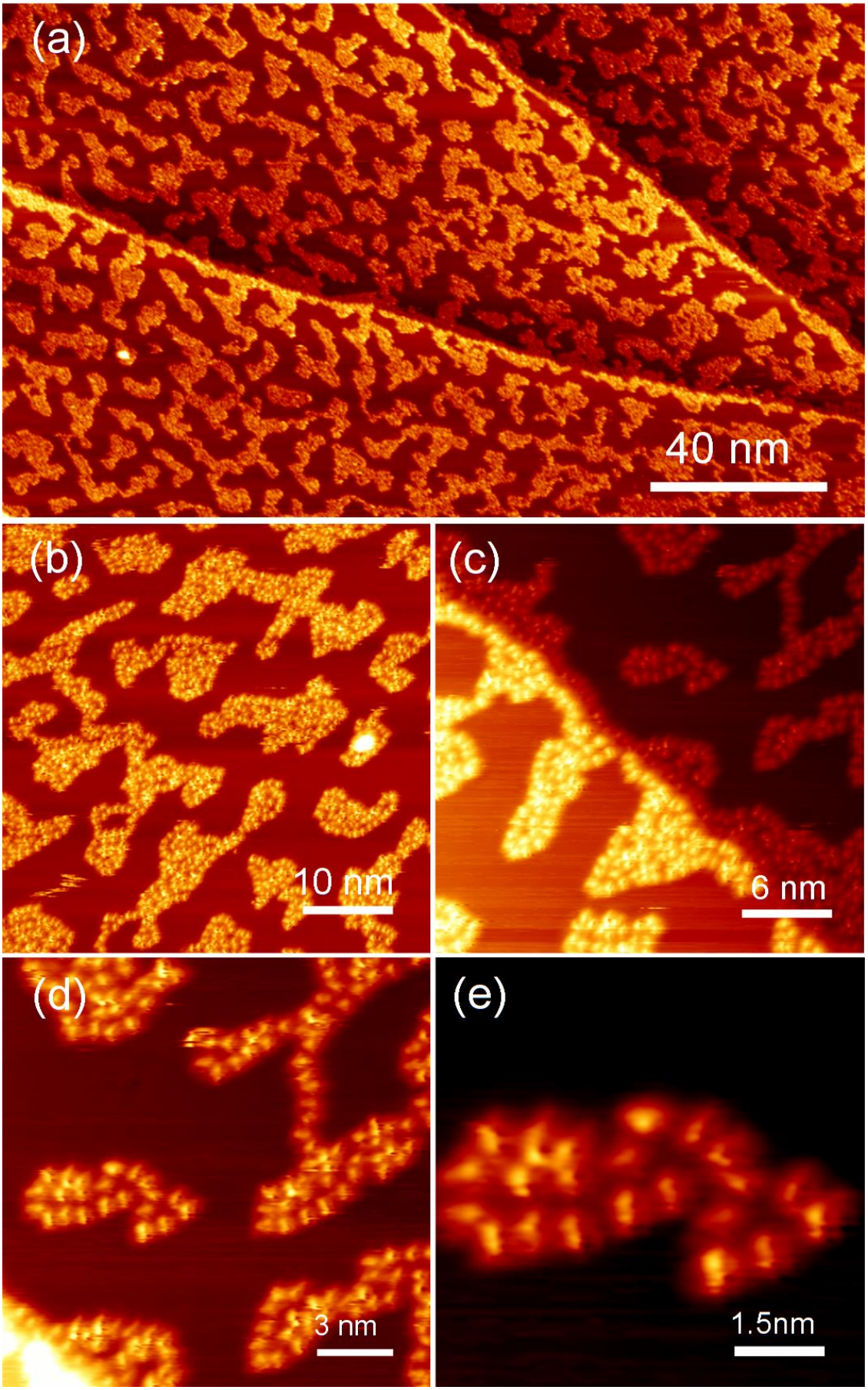

Figure 1. STM images recorded upon vapor deposition of (sub-)monolayer amounts of [BMP][TFSA] on a Cu(111) substrate held at ~200 K and subsequent cool down to ~100 K. The large-scale STM image in (a) shows islands with relaxed dendritic shapes (U_t=+1.5 V, I_t=15 pA). Figures (b) and (c) resolve that the islands consist of aggregated protrusions which are arranged in a disordered manner (U_t=+1.5 V, I_t=15 pA). The small-scale STM image in Figure (d) and (e) reveal that the protrusions appear either roundish or elliptical (U_t=+1.5 V, I_t=15 pA)

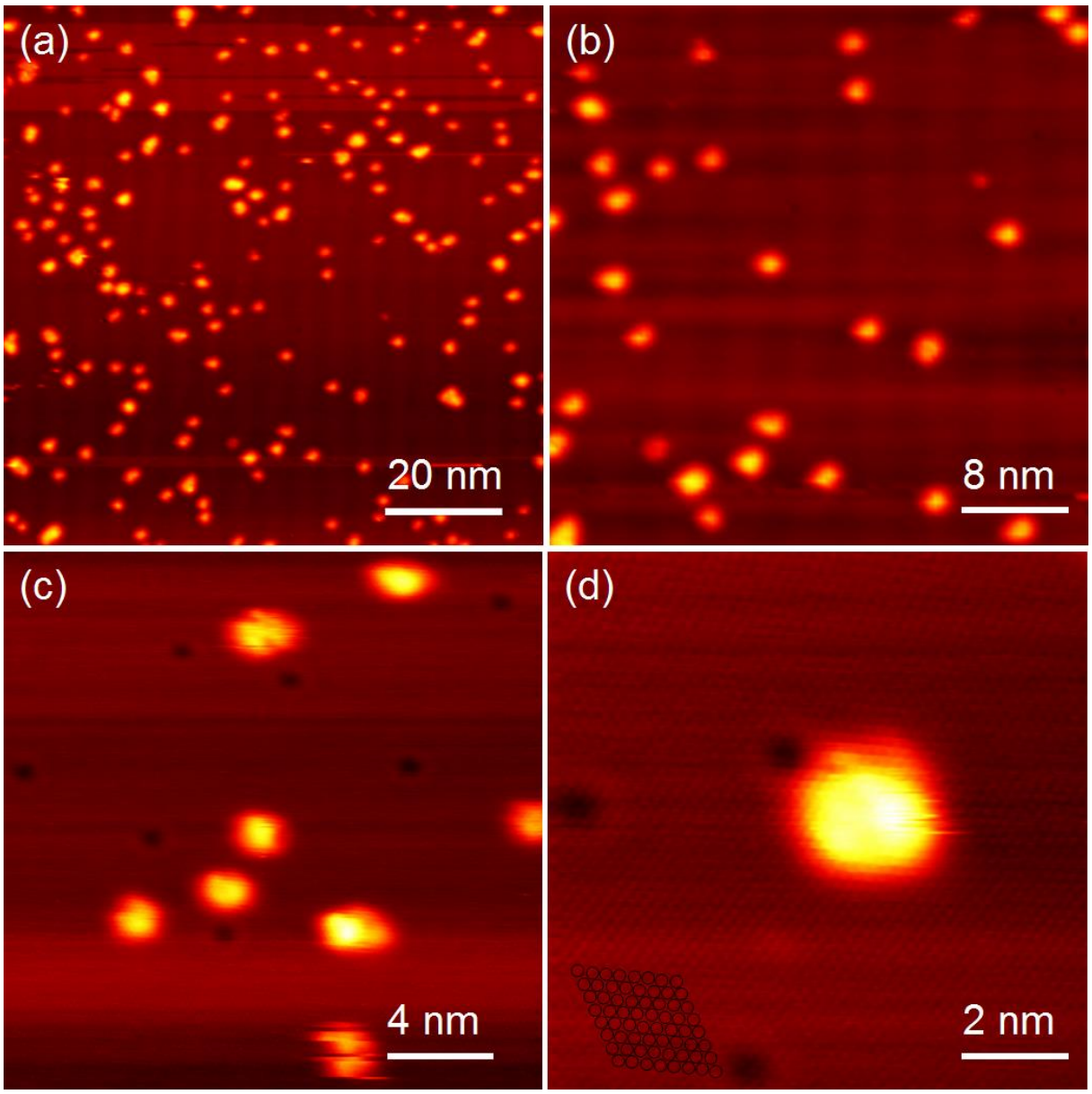

Figure 2. STM images of adsorbed Li on a Cu(111). After Li was vapor deposited on the sample held at 80 K the STM measurements were carried out at ~100 K. (a) and (b) The large-scale STM image shows individual protrusions (U_t=+1.0 V, I_t=20 pA). Figure (c) shows a magnified STM image; in the small-scale STM image in Figure (d) the copper atomic lattice is resolved. (U_t=+0.5 V, I_t=30 pA).

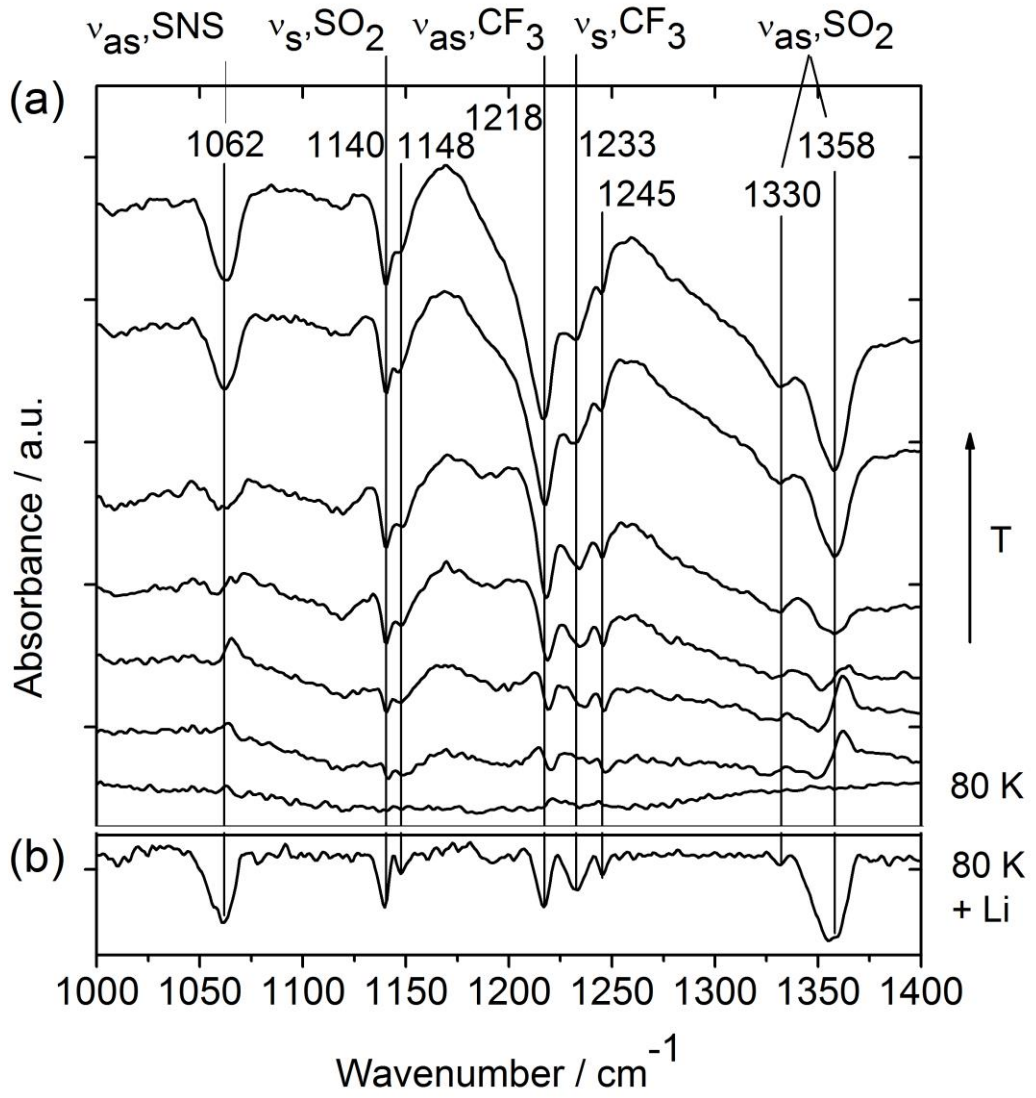

Figure 3. (a) FTIR difference spectra recorded after vapor deposition of multilayers of [BMP][TFSA] on a Cu(111) substrate held at 80 K (~ 6 ML) and subsequent slow annealing, showing the spectral range between 1000 cm^{-1} and 1400 cm^{-1} with the vibrational modes of the anion (background: spectrum recorded upon deposition at 80 K). (b) After vapor deposition of the same amount of [BMP][TFSA] on a clean Cu(111) held at 80 K and subsequent Li co–deposition the FTIRS difference spectrum displays the same changes in the vibrational modes.

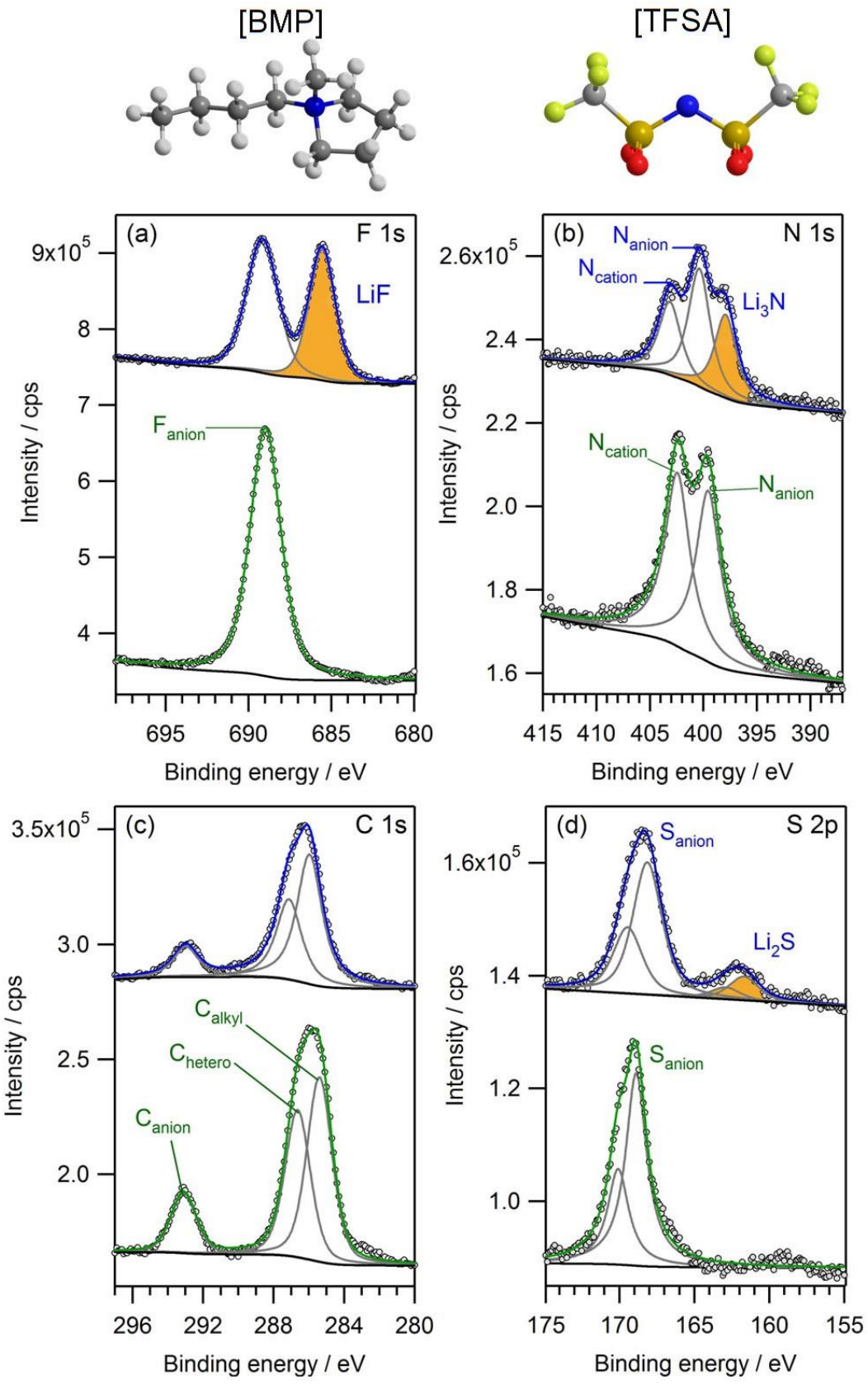

Figure 4. XP spectra recorded after vapor deposition of multilayers of [BMP][TFSA] on a Cu(111) substrate held at 80 K (~ 6 ML) (bottom) and upon post–deposition of Li (top).

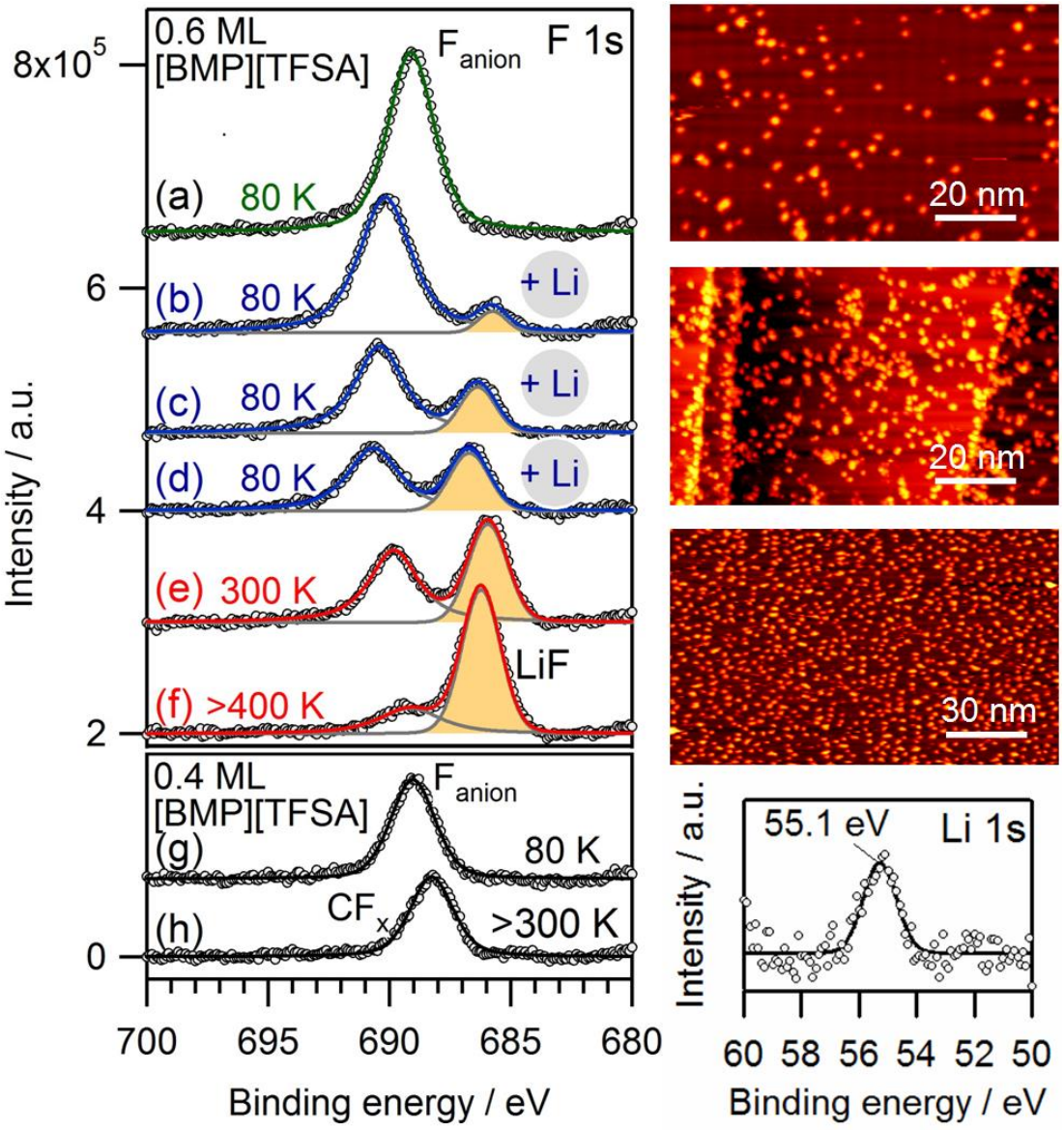

Figure 5. XP spectra of the F 1s region after vapor deposition of 0.6 ML of [BMP][TFSA] on a Cu(111) substrate held at 80 K (a) and successive post–deposition of small amounts of Li (b–d). STM images next to the spectra show Cu(111) surfaces at 80 K after vapor deposition of the corresponding amounts of Li on clean Cu(111) (particle densities ρ_{Li} were evaluated to ρ_{Li} = 0.02 nm^{-2}, ρ_{Li} = 0.05 nm^{-2} and ρ_{Li} = 0.07 nm^{-2}.) (U_t=+1.0 V, I_t=20 pA (top), U_t=+2.1 V, I_t=50 pA, (middle), U_t=+1.3 V, I_t=20 pA (bottom)). The XP spectrum corresponding to the lower STM image shows a small peak related to adsorbed Li. Subsequently the sample was heated to room temperature (e) and to around 450 K (f). For comparison, we also show XP spectra recorded after similar treatment on Li-free adlayer covered surfaces in (g) and (h).

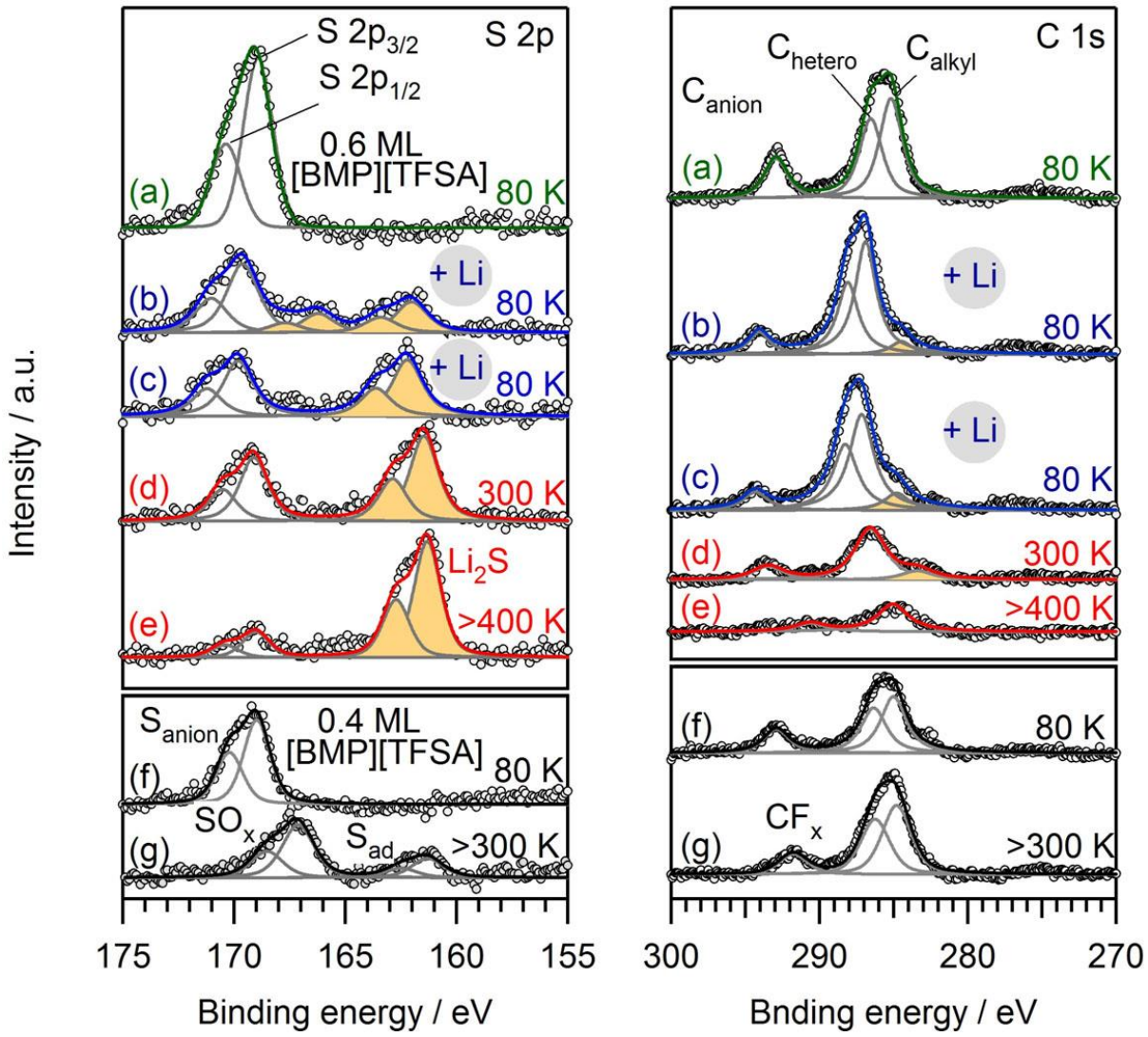

Figure 6. XP spectra of the S 2p and C 1s regions, respectively, after vapor deposition of 0.6 ML of [BMP][TFSA] on a Cu(111) substrate held at 80 K (a) and after successive co–deposition of small amounts of Li (b–c). Subsequently the sample was heated to room temperature (d) and to around 450 K (e) and XPS was performed at the given temperatures. For a comparison of the temperature–dependent behavior XP spectra recorded without addition of Li are shown in (f) and (g).

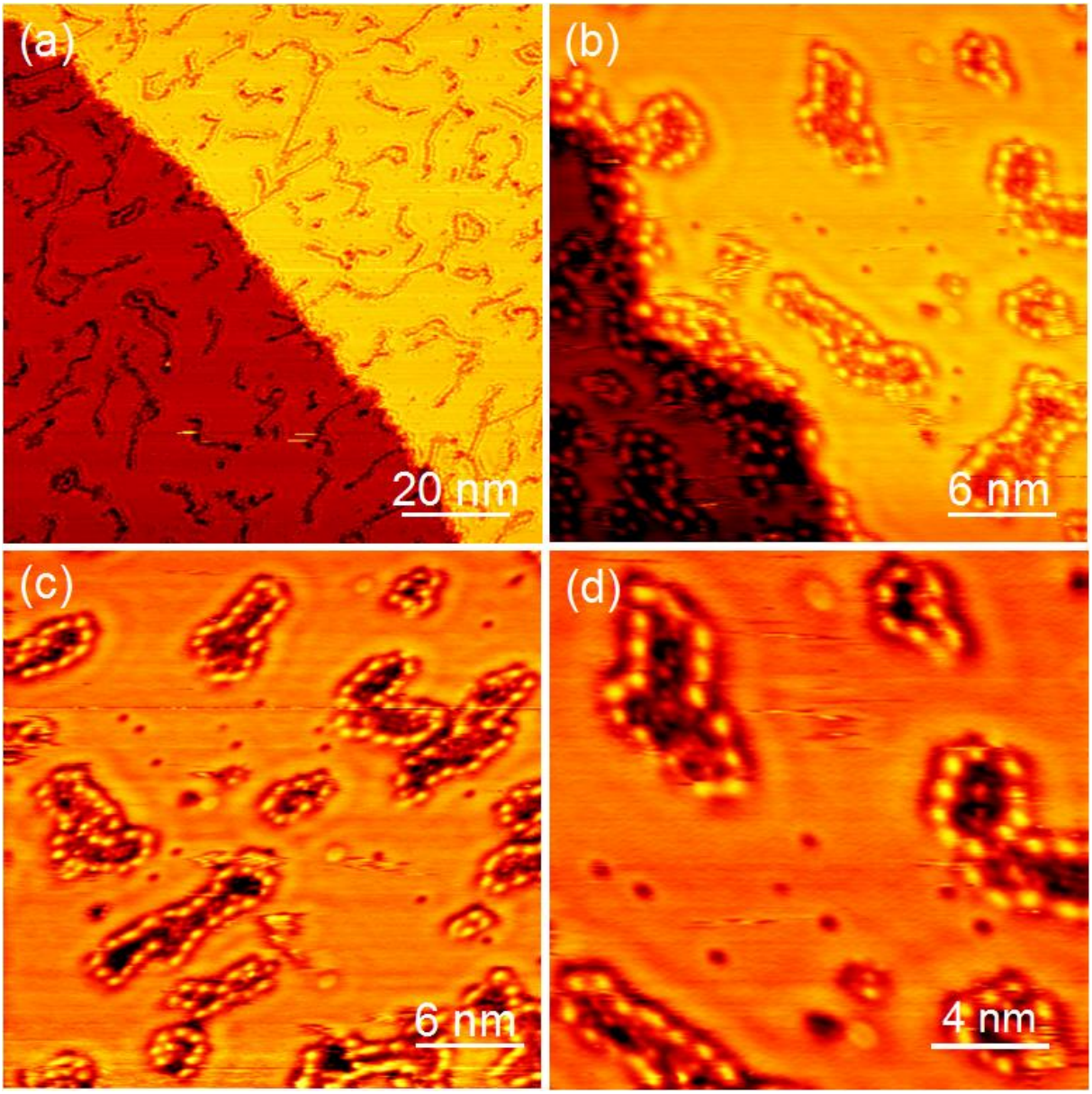

Figure 7. (a) Large–scale STM image of the adsorption structure after vapor deposition of [BMP][TFSA] and subsequent co–deposition of Li on Cu(111) at around 100 K (U_t=+1.3 V, I_t=20 pA). (b–d) High–resolution STM images of the same surface, resolving the islands as areas with a lower apparent height, which are decorated by a sequence of protrusions at the boundaries (U_t=+1.3 V, I_t=30 pA). Islands are observed also at the ascending and descending side of the step edges in Figure (b). In Figures (c) and (d), additional molecular features are visible inside the islands.

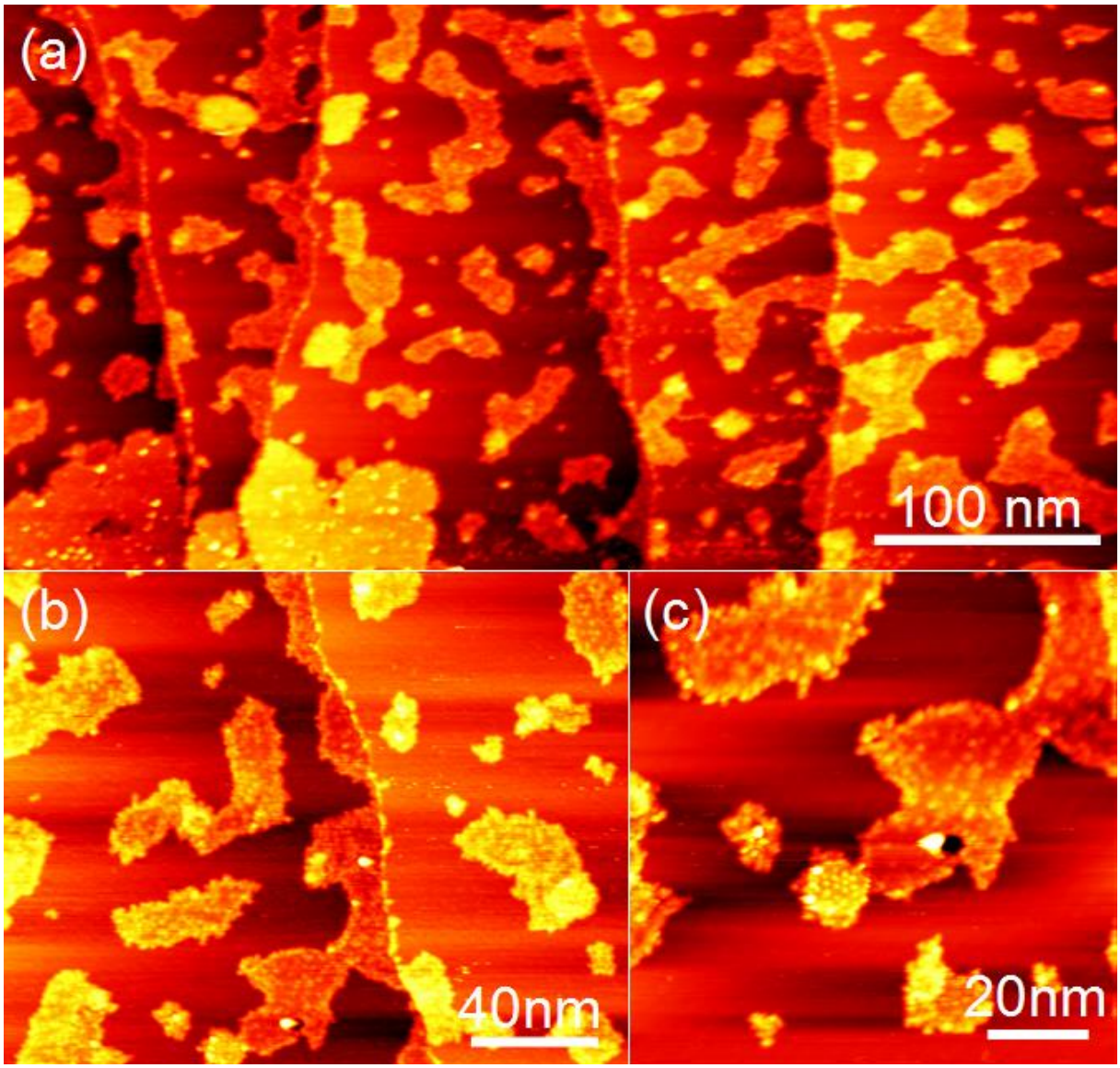

Figure 8. (a) Large-scale STM images (500 nm × 500 nm) (a), (200 nm × 200 nm) (b) and (100 nm × 100 nm) (c), recorded after vapor deposition of [BMP][TFSA] on Cu(111) held at 100 K, subsequent co–deposition of Li, heating to around 450 K and final cool down to 100 K (U_t=–0.33 V, I_t=150 pA).

Notes

The authors declare no competing financial interest.

ACKNOWLEDGEMENT

This work was supported by the Bundesministerium für Bildung und Forschung in the project LiEcoSafe under contract number 03X4636C. B.U. gratefully acknowledges a fellowship by the Fonds der Chemischen Industrie.

Supporting Information Available. This material is available free of charge *via* the Internet a http://pubs.acs.org

REFERENCES

1. Welton, T. Room-Temperature Ionic Liquids. Solvents for Synthesis and Catalysis. *Chem. Rev.* **1999,** *99*, 2071-2084.

2. Wasserscheid, P.; Keim, W. Ionic Liquids—New "Solutions" for Transition Metal Catalysis. *Angew. Chem. Int. Ed.* **2000,** *39*, 3772-3789.

3. Plechkova, N. V.; Seddon, K. R. Applications of Ionic Liquids in the Chemical Industry. *Chem. Soc. Rev.* **2008,** *37*, 123-150.

4. Smiglak, M.; Pringle, J. M.; Lu, X.; Han, L.; Zhang, S.; Gao, H.; MacFarlane, D. R.;Rogers, R. D. Ionic Liquids for Energy, Materials, and Medicine. *Chem. Commun. Chem.Commun*. **2014**, *50*, 9228-9250.

5. Armand, M.; Tarascon, J.–M. Building Better Batteries. *Nature* **2008,** *451*, 652–657.

6. Armand, M.; Endres, F.; MacFarlane, D. R.; Ohno, H.; Scrosati, B. Ionic–liquid Materials for the Electrochemical Challenges of the Future. *Nature Mater.* **2009,** *8*, 621–629.

7. Girishkumar, G.; McCloskey, B.; Luntz, A. C.; Swanson, S.; Wilcke, W. Lithium–Air Battery: Promise and Challenges. *J. Phys. Chem. Lett.* **2010,** *1*, 2193–2203.

8. Atkin, R.; El Abedin, S. Z.; Hayes, R.; Gasparotto, L. H. S.; Borisenko, N.; Endres, F. AFM and STM Studies on the Surface Interaction of [BMP]TFSA and [EMIm]TFSA Ionic Liquids with Au(111). *J. Phys. Chem. C* **2009,** *113*, 13266–13272.

9. Endres, F.; Höfft, O.; Borisenko, N.; Gasparotto, L. H. S.; Prowald, A.; Al Salman, R.; Carstens, T.; Atkin, R.; Bund, A.; El Abedin, S. Z. Do Solvation Layers of Ionic Liquids Influence Electrochemical Reactions? *Phys. Chem. Chem. Phys.* **2010,** *12*, 1724–1732.

10. Atkin, R.; Borisenko, N.; Drüschler, M.; El Abedin, S. Z.; Endres, F.; Hayes, R.; Huber, B.; Roling, B. An *in Situ* STM/AFM and Impedance Spectroscopy Study of the Extremely Pure 1–Butyl–1–Methylpyrrolidinium Tris(pentafluoroethyl)trifluorophosphate/Au(111) Int erface: Potential Dependent Solvation Layers and the Herringbone Reconstruction. *Phys. Chem. Chem. Phys.* **2011,** *13*, 6849–6857.

11. Drüschler, M.; Borisenko, N.; Wallauer, J.; Winter, C.; Huber, B.; Endres, F.; Roling, B. New Insights into the Interface between a Single–Crystalline Metal Electrode and an Extremely Pure Ionic Liquid: Slow Interfacial Processes and the Influence of Temperature on Interfacial Dynamics. *Phys. Chem. Chem. Phys.* **2012,** *14*, 5090–5099.

12. Gnahm, M.; Berger, C.; Arkhipova, M.; Kunkel, H.; Pajkossy, T.; Maas, G.; Kolb, D. M. The Interfaces of Au(111) and Au(100) in a Hexaalkyl–Substituted Guanidinium Ionic Liquid: an Electrochemical and *in Situ* STM Study. *Phys. Chem. Chem. Phys.* **2012,** *14*, 10647–10652.

13. Müller, C.; Vesztergom, S.; Pajkossy, T.; Jacob, T. The Interface between Au(100) and 1–butyl–3–methyl–imidazoliumbis(trifluoromethylsulfonyl)imide. *J. Electroanal. Chem.* **2015**, *737*, 218–225.

14. Steinrück, H.–P.; Libuda, J.; Wasserscheid, P.; Cremer, T.; Kolbeck, C.; Laurin, M.; Maier, F.; Sobota, M.; Schulz, P. S.; Stark, M. Surface Science and Model Catalysis with Ionic Liquid–Modified Materials . *Adv. Mater.* **2011,** *23*, 2571–2587.

15. Steinrück, H.–P. Recent Developments in the Study of Ionic Liquid Interfaces Using X–ray Photoelectron Spectroscopy and Potential Future Directions. *Phys. Chem. Chem. Phys.* **2012,** *14*, 5010–5029.

16. Höfft, O.; Bahr, S.; Himmerlich, M.; Krischok, S.; Schaefer, J. A.; Kempter, V. Electronic Structure of the Surface of the Ionic Liquid [EMIM][Tf_2N] Studied by Metastable Impact Electron Spectroscopy (MIES), UPS, and XPS. *Langmuir* **2006,** *22*, 7120–7123.

17. Maier, F.; Gottfried, J. M.; Rossa, J.; Gerhard, D.; Schulz, P. S.; Schwieger, W.; Wasserscheid, P.; Steinrück, H.–P. Surface Enrichment and Depletion Effects of Ions Dissolved in an Ionic Liquid: An X–Ray Photoelectron Spectroscopy Study. *Angew. Chem. Int. Ed.* **2006,** *45*, 7778–7780.

18. Lovelock, K. R. J.; Villar–Garcia, I. J.; Maier, F.; Steinrück, H. P.; Licence, P. Photoelectron Spectroscopy of Ionic Liquid–Based Interfaces. *Chem. Rev.* **2010,** *110*, 5158–5190.

19. Schernich, S.; Laurin, M.; Lykhach, Y.; Steinrück, H.–P.; Tsud, N.; Skála, T.; Prince, K. C.; Taccardi, N.; Matolín, V.; Wasserscheid, P.; *et al.* Functionalization of Oxide Surfaces through Reaction with 1,3–Dialkylimidazolium Ionic Liquids. *J. Phys. Chem. Lett.* **2012,** *4*, 30–35.

20. Cremer, T.; Stark, M.; Deyko, A.; Steinrück, H.–P.; Maier, F. Liquid/Solid Interface of Ultrathin Ionic Liquid Films: [C_1C_1Im][Tf_2N] and [C_8C_1Im][Tf_2N] on Au(111). *Langmuir* **2011,** *27*, 3662–3671.

21. Foulston, R.; Gangopadhyay, S.; Chiutu, C.; Moriarty, P.; Jones, R. G. Mono– and Multi–Layer Adsorption of an Ionic Liquid on Au(110). *Phys. Chem. Chem. Phys.* **2012,** *14*, 6054–6066.

22. Waldmann, T.; Huang, H.–H.; Hoster, H. E.; Höfft, O.; Endres, F.; Behm, R. J. Imaging an Ionic Liquid Adlayer by Scanning Tunneling Microscopy at the Solid | Vacuum Interface. *ChemPhysChem* **2011,** *12*, 2565–2567.

23. Buchner, F.; Forster–Tonigformer, K.; Uhl, B.; Alwast, D.; Wagner, N.; Farkhondeh, H.; Groß, A.; Behm, R. J. Toward the Microscopic Identification of Anions and Cations at the Ionic Liquid|Ag(111) Interface: A Combined Experimental and Theoretical Investigation. *ACS Nano*, **2013**, *7*, 7773–7784.

24. Uhl, B.; Cremer, T.; Roos, M.; Maier, F.; Steinrück, H.–P.; Behm, R. J. At the Ionic Liquid|Metal Interface: Structure Formation and Temperature Dependent Behavior of an Ionic Liquid Adlayer on Au(111). *Phys. Chem. Chem. Phys.*, **2013**, *15*, 17295–17302.

25. Uhl, B.; Buchner, F.; Alwast, D.; Wagner, N.; Behm, R. J. Adsorption of the Ionic Liquid [BMP][TFSA] on Au(111) and Ag(111): Substrate Effects on the Structure Formation Investigated by STM. *Beilstein J. Nanotechnol.* **2013**, *4,* 903–918.

26. Uhl, B.; Buchner, F.; Gabler, S.; Bozorgchenani, M.; Behm, R. J. Adsorption and Reaction of Sub–monolayer Films of an Ionic Liquid on Cu(111). *Chem. Commun.* **2014**, *50*, 8601–8604.

27. Verma, P.; Maire, P.; Novak, P. A Review of the Features and Analyses of the Solid Electrolyte Interphase in Li–ion Batteries. *Electrochim. Acta*, **2010**, *55*, 6332–6341.

28. Kurisaki, T.; Tanaka, D.; Inoue, Y.; Wakita, H.; Minofar, B.; Fukuda, S.; Ishiguro, S.–i.; Umebayashi, Y. Surface Analysis of Ionic Liquids with and without Lithium Salt Using X–ray Photoelectron Spectroscopy. *J. Phys. Chem. B*, **2012**, *116*, 10870–10875.

29. Olschewski, M. , Gustus, R., Marschewski, M., Höfft, O., Endres, F. Spectroscopic Characterization of the Interaction of Lithium with Thin Films of the Ionic Liquid 1-octyl-3-methyl-imidazolium bis-(tri-fluoro-methyl-sulfonyl)amide, *Phys.Chem.Chem.Phys*. **2014**, 16, 25969–25977.

30. Ismail, I.; Noda, A.; Nishimoto, A.; Watanabe, M. XPS Study of Lithium Surface after Contact with Lithium–salt Doped Polymer Electrolytes. *Electrochimica Acta* **2001**, *46*, 1595–1603.

31. Xu, C.; Sun, B.; Gustafsson, T.; Edström, K.M; Brandell, D.; Hahlin, M. Interface Layer Formation in Solid Polymer Electrolyte Lithium Batteries: an XPS Study. *J. Mater. Chem. A* **2014**, *2*, 7256–7264.

32. Aurbach, D.; Zaban, A.; Ein–Eli, Y.; Weissman, I.; Chusid, O.; Markovsky, B.; Levi, M.; Levi, E.; Schechter, A.; Granot, E. Recent Studies on the Correlation between Surface Chemistry, Morphology, Three–dimensional Structures and Performance of Li and Li–C Intercalation Anodes in Several Important Electrolyte systems. *J. Power Sources* **1997**, *68*, 91–98.

33. Nguyen, C. C.; Song, S.–W. Characterization of SEI Layer Formed on High Performance Si–Cu Anode in Ionic Liquid Battery Electrolyte. *Electrochem. Commun*. **2010**, *12*, 1593–1595.

34. Buchner, F.; Farkhondeh, H.; Bozorgchenani, M.; Uhl, B.; Behm, R. J. Temperature–induced Structural and Chemical Changes of Ultrathin Ethylene Carbonate Films on Cu(111). *Phys. Chem. Chem. Phys.* **2014**, *16*, 11191–11195.

35. Simic–Milosevic, V.; Heyde, M.; Nilius, N.; Nowicki, M.; Rust, H.–P.; Freund, H.–J. Substrate-mediated Interaction and Electron-induced Diffusion of Single Lithium Atoms on Ag(001*). Phys. Rev. B* **2007**, *75*, 195416–5.

36. Krull, C.; Robles, R.; Mugarza, A; Gambardella, P. Site- and Orbital-dependent Charge Donation and Spin Manipulation in Electron-doped Metal Phthalocyanines. *Nature Materials* **2013**, *12*, 337–343.

37. Sobota, M.; Nikiforidis, I.; Hieringer, W.; Paape, N.; Happel, M.; Steinrück, H.–P.; Görling, A.; Wasserscheid, P.; Laurin, M.; Libuda, J. Toward Ionic–Liquid–Based Model Catalysis: Growth, Orientation, Conformation, and Interaction Mechanism of the [Tf_2N] Anion in [BMIM][Tf_2N] Thin Films on a Well–Ordered Alumina Surface. *Langmuir* **2010,** *26*, 7199–7207.

38. Sobota, M.; Schmid, M.; Happel, M.; Amende, M.; Maier, F.; Steinrück, H.–P.; Paape, N.; Wasserscheid, P.; Laurin, M.; Gottfried, J. M.; *et al*. Ionic Liquid Based Model Catalysis: Interaction of [BMIM][Tf_2N] with Pd Nanoparticles Supported on an Ordered Alumina Film. *Phys. Chem. Chem. Phys.* **2010,** *12*, 10610–10621.

39. Rey, I.; Johansson, P.; Lindgren, J.; Lasségues, J. C.; Grondin, J.; Servant, L. J. Spectroscopic and Theoretical Study of $(CF_3SO_2)_2N$- (TFSI-) and $(CF_3SO_2)_2NH$ (HTFSI). *Phys. Chem. A* **1998**, *102*, 3249–3258.

40. Höfft, O.; Bahr, S.; Kempter, V. Investigations with Infrared Spectroscopy on Films of the Ionic Liquid [EMIM]Tf2N. *Langmuir* **2008**, *24*, 11562–11566.

41. Morgan, W. E.; Van Wazer, J. R.; Stec, W. J. Inner–Orbital Photoelectron Spectroscopy of the Alkali Metal Halides, Perchlorates, Phosphates, and Pyrophosphates. *J. Am. Chem. Soc*. 1973, **95**, 751–755.

42. Diao, Y.; Xie, K., Xiong, S.; and. Hong, X; Insights into Li-S Battery Cathode Capacity Fading Mechanism: Irreversible Oxidation of Active Mass during Cyling. *J. Electrochem. Soc*. **2012**, *159*, A1816–A1821.

43. Shek, M.L.; Hrbek, J.; Sham, T.K.; Xu, G.Q. A Soft X-Ray Study of the Interaction of Oxygen with Li. *Surf. Sci.* **1990**, *234*, 324–334.

44. Streber, R.; Papp, C.; Lorenz, M. P. A.; Bayer, A.; Denecke, R.; Steinrück, H.-P. Sulfur Oxidation on Pt(355): It is the Steps! *Angew. Chem. Int. Ed.* **2009**, *48*, 9743 – 9746.

45. Plocik, M.; Wilde, L.; Haase, J.; Brena, B.; Cocco, D.; Comelli, G.; Paolucci, G. Adsorption and Temperature-dependent Decomposition of SO_2 on Cu(100) and Cu(111). A Fast and High-resolution Core-level Spectroscopy Study. *Phys. Rev. B* **1996**, *53*, 13720–13724.

46. Aurbach, D.; Pollak E.; Elazari, R.; Salitra, G.; Kelley, C. S.; Affinito, J. On the Surface Chemical Aspects of Very High Energy Density, Rechargeable Li–Sulfur Batteries. *J. Electrochem. Soc*. **2009**, *156 (8),* A694-A702.

47. Schmid, M.; Steinrück, H.-P.; Gottfried, J.M. A New Asymmetric Pseudo-Voigt Function for More Efficient Fitting of XPS Lines. *Surf. Interface Anal.* **2014**, *46*, 505–511.

BRIEFS

STM images of [BMP][TFSA] and lithium adsorbed on Cu(111) at 80 K, respectively, and after co–adsorption of both components. The XP spectra reveal the formation of a new adspecies (LiF) upon post–deposition of increasing amounts of lithium.

SYNOPSIS